ELSEVIER

PII: S0032-3861(97)00352-2

Polymer Vol. 39 No. 3, pp. 651–658, 1998

0032-3861/97/$17.00+0.00

Temperature–concentration diagram of polystyrene-*block*-polydimethylsiloxane associates formed in dilute solution of selective solvent

Kayori Iyama and Takuhei Nose*

Department of Polymer Chemistry, Tokyo Institute of Technology, 2-12-1 Ookayama, Meguro-ku, Tokyo 152, Japan

(Received 14 February 1997; revised 2 April 1997; accepted 21 April 1997)

Association behaviour of polystyrene-*block*-polydimethylsiloxane (PS-*block*-PDMS) in dilute solution of selective solvent is investigated by static and dynamic light-scattering as a function of temperature and concentration. Number-average molecular weights of PS and PDMS blocks are 7.8×10^3 g mol^{-1} and 3.2×10^3 g mol^{-1}, respectively, and the solvent is a mixture of *n*-octane (C8) and methylcyclohexane (MCH) with the compositions of C8/MCH = 1.23 by weight, which is selective for PDMS. On heating the solutions from 12°C to 72°C, three different micellar regions are observed over a concentration range of 10^{-4}–10^{-2} g (g of solution)$^{-1}$. The highest temperature region right below the unimer region is the so-called anomalous-micellization region, where large spherical particles are formed and grow, and eventually precipitate in a few days. In the second region at intermediate temperatures, hollow spherical micelles (vesicles) are formed with large association numbers of about 10^3. The third region is located at low temperatures and low polymer concentrations, where hollow cylindrical micelles with the estimated length/diameter ratio of less than 16 are formed. These hollow cylindrical micelles are observed on heating only, but not on cooling from the unimer region, so they are presumed not to be in equilibrium state but to be meta-stable micelles formed on micellization processes. © 1997 Elsevier Science Ltd.

(Keywords: micelle; block copolymer; light-scattering)

INTRODUCTION

Micellization of block copolymers in selective solvent has been studied to a large extent in view of a wide variety of micellar structures and phase behaviour of these solutions by using static and dynamic light-scattering and other experimental techniques[1–4]. Theoretical and experimental studies have demonstrated that micellization of diblock copolymers is essentially the closed association[5], having critical micelle temperature (c.m.t.) and critical micelle concentration (c.m.c.)[6]. Zhou *et al.*[7] studied the change of unimer and micelle concentrations near c.m.c. on the temperature-induced associating behaviour of polystyrene-*block*-poly(*tert*-butylstyrene) in *N,N*-dimethylacetamide. Quintana *et al.*[8,9] measured the temperature dependence of c.m.c. for micelle formation of polystyrene-*block*-poly (ethylene/propylene) in *n*-dodecane/1,4-dioxane mixtures and evaluated some thermodynamic functions. Honda *et al.*[10] made an investigation of relationships between the solvent quality and the change of association number and micelle-forming fraction near c.m.c. for poly(α-methylstyrene)-*block*-poly(vinyl-*p*-phenethyl alcohol) in *m*-chlorobenzyl chloride/*m*-chlorobenzyl alcohol mixtures. Gao and Eisenberg[11] studied the c.m.c. of polydisperse diblock copolymers, which was called a mixed critical micelle concentration (c.m.c.[mix]). All these investigations have revealed that the c.m.t. decreases with decreasing concentration and that the association number monotonically increases with distance from the c.m.c. and/or the c.m.t.

On the other hand, micellar solutions of certain diblock copolymers in selective solvents exhibit phase behaviour different from these simple behaviours[12–25]. Tsunashima and co-workers[12,13] observed a double-step transition of the diffusion coefficient for polystyrene-*block*-polybutadiene (PS-*block*-PB) in *n*-decane as the concentration increased from 3.8×10^{-6} g cm^{-3} to 1.1×10^{-4} g cm^{-3}. At an extremely dilute concentration ($C < 3.8 \times 10^{-6}$ g cm^{-3}) PS-*block*-PB was molecularly dispersed, and formed spherical micelles at higher concentrations ($C > 1.1 \times 10^{-4}$ g cm^{-3}). At an intermediate concentration (3.8×10^{-6} g cm$^{-3} < C < 1.1 \times 10^{-4}$ g cm^{-3}), they observed a unique diffusion which is slower than that observed in the spherical micelle region, suggesting formation of different micelles. For aqueous solution of poly(ethylene oxide)-*block*-poly(propylene oxide)-*block*-poly(ethylene oxide), very complex phase behaviours were reported[14–25]: Micellar structure changes from spherical to prolate ellipsoid or rod-like form as concentration and/or temperature increase, and in some cases an opalescence or a precipitate appear in the transitional region of temperatures near the c.m.t., which is the so-called anomalous micellization. Sikora and Karasz[25] theoretically investigated a temperature–concentration diagram of micellar solutions, and showed that an immiscibility regime could be expected in the transitional region between molecular and micellar block copolymer solutions. The phase behaviours of micellar solutions near the c.m.c. are so complex that general rules for the behaviour have not been established yet.

In this series of studies, we investigate the association

* To whom correspondence should be addressed

phenomena and phase behaviour of PS-*block*-PDMS in selective solvent near the transitional region between unimers and micelles as a function of temperature and concentration using static and dynamic light-scattering. To achieve this purpose, we used a mixed solvent composed of *n*-octane, strongly selective for PDMS, and methylcyclohexane, weakly selective for PDMS, and chose the composition of the mixture so that micelle formation, decomposition and rearrangement can be observed in measurable temperature and concentration ranges. In this mixed solvent PS-*block*-PDMS forms micelles having a core of PS and a corona of PDMS. We measured static and dynamic properties of the solutions as a function of temperature for different concentrations and found three characteristic temperature–concentration regions. Spherical micelles are formed in one region, and cylindrical micelles with large association number appear in another region at lower temperatures and concentrations. The remaining region is the anomalous-micellization region at higher temperatures bordering on the spherical-micelle region and the unimer region. In this paper, we demonstrate detailed micellar structures and the association behaviour of this copolymer solution to present a temperature–concentration diagram peculiar to diblock-copolymer micellar solutions in selective solvent near c.m.c. and/or c.m.t.

EXPERIMENTAL

Materials

PS-*block*-PDMS was synthesized by anionic polymerization. Number-average molecular weights of PS and PDMS blocks were 7.8×10^3 g mol^{-1} and 3.2×10^3 g mol^{-1}, respectively, and the molecular-weight distribution index *Mw/Mn* of PS-*block*-PDMS was 1.18. The solvent was a mixture of *n*-octane (C8) and methylcyclohexane (MCH) with the composition of C8/MCH = 1.23 by weight. Purchased C8 and MCH were dried over calcium hydride and purified by fractional distillation before use. For determination of association properties and structure by light-scattering, the combination of C8 and MCH as components of the mixed solvent has the advantage that no strong preferential adsorption is expected because of good miscibility with each other and similar selectivity for PS-*block*-PDMS, and that C8, MCH and PDMS are isorefractive with each other.

Light-scattering measurement

The light-scattering apparatus was a standard, laboratory-built one with an Ar–ion laser operating at 488 nm as a light source using a photon-counting method. The temperature was controlled to within ± 0.01°C. Static light-scattering measurements were performed at angles between 30° and 120°. The auto-correlation function of scattered-light intensity was measured with a Kowa digital correlator of 56 channels.

Stock solution with the concentration of 1×10^{-2} g (g of solution)$^{-1}$ was prepared by dissolving the block copolymer in the mixed solvent, and keeping the solution at 85°C for 1 h and at room temperature for 1 day with mild stirring. The stock solution was filtered through a Millipore filter with nominal pore size of 0.5 μm into a dust-free optical cell at room temperature and diluted, with solvent filtered through a Millipore filter with nominal pore size of 0.2 μm, to the desired concentration. The optical cells were flame-sealed under mild vacuum.

Excess Rayleigh ratio $\Delta R(\theta)$ was calculated from the measured excess scattered-light intensity using the intensity of benzene as standard. The Rayleigh ratio of benzene at an angle of 90°, used as a standard, was given as a function of temperature t in °C as follows[26–28]:

$$R_{vv}^{B}(90°) = 3.20 \times 10^{-5}\left[1 + 3.68 \times 10^{-3}(t - 25)\right] \quad (1)$$

The obtained excess Rayleigh ratio, as a function of scattering angle θ and concentration C (g ml^{-1}), was described by

$$\frac{KC}{\Delta R(\theta)} = \frac{1}{M_w}\left[1 + \frac{16\pi^2 n^2}{3\lambda^2} R_g^2 \sin^2\left\{\frac{\theta}{2}\right\}\right] + 2A_2 C + \cdots \quad (2)$$

where M_w, R_g^2 and A_2 are weight-average molecular weight, z-average mean square radius of gyration and the second virial coefficient, respectively. K is the optical constant defined by

$$K = \frac{4\pi^2 n^2 (dn/dC)^2}{\lambda^4 N_A} \quad (3)$$

where n, λ and N_A are the refractive index of the solvent, the wavelength of incident beam and Avogadro constant, respectively. The refractive-index increment *dn/dC* was measured by a differential refractometer (Union Giken RM-102) with a He–Ne laser of 633 nm being used as light source. Light-scattering measurements were carried out with the light source at 488 nm, but measured values of scattered-light intensity at zero-angle with the two different light sources were equal within experimental error. This implies that $(dn/dC)^2 n^2 \lambda^{-4}$ is practically the same for both light sources. M_w, R_g and A_2 were determined by Zimm plots on the basis of equation (2). Since the refractive index of the solvent is almost equal to that of PDMS, the obtained R_g can be regarded as that of the PS part of a micelle.

The above conventional analysis could not be applied to some temperature–concentration conditions because there occurred changes in the phase behaviour and the association properties of diblock copolymers with concentration. In these cases we evaluated apparent molecular weight M_{wapp} and apparent radius of gyration R_{gapp} without the extrapolation, which were defined as

$$M_{wapp} = \frac{\Delta R(0)}{KC} \quad (4)$$

$$R_{gapp}^2 = \frac{3\lambda^2 M_{wapp}(\textit{initial slope})}{16\pi^2 n^2} \quad (5)$$

$KC/\Delta R(0)$ and (*initial slope*) are the intercept and the initial slope in the plot of $KC/\Delta R(0)$ *versus* $\sin^2(\theta/2)$ at finite concentrations.

The correlation function of electric field obtained from the auto-correlation function of scattered-light intensity was analyzed by a cumulant method. Namely, from the non-linear least-squares fitting to the cumulant expansion

$$\left|g^{(1)}(\tau)\right| = \exp(-\bar{\Gamma}\tau + \frac{1}{2}\mu_2\tau^2 - \cdots) \quad (6)$$

we evaluated the average decay rate $\bar{\Gamma}$ and the second cumulant μ_2. The $\bar{\Gamma}$ value followed the q^2 dependence, i.e. $\bar{\Gamma} = Dq^2$, under the condition of $R_g q \leq 1$, where q is defined as $q = (4\pi n/\lambda)\sin(\theta/2)$. Dynamic light-scattering measurements were performed at an angle of 30° under the condition

of $R_g q \leq 1$ except for a few cases when R_g was extremely large. The diffusion coefficient D calculated from $\bar{\Gamma}$ as a function of concentration C was extrapolated to infinite dilution to obtain the diffusion coefficient D_0 at $C = 0$. Hydrodynamic radius R_h was calculated by the Einstein–Stokes equation

$$R_h = \frac{k_B T}{6\pi\eta D_0} \tag{7}$$

where k_B, T and η are the Boltzman constant, absolute temperature and solvent viscosity, respectively. The solvent viscosity η was measured by a Ubbelohde-type viscometer as a function of temperature. Similarly to M_w and R_g, extrapolations to zero concentration were not possible in some cases, so in these cases the R_h was replaced by the apparent hydrodynamic radius R_{happ} at the finite concentration without extrapolation.

Within the experimental range of the concentration, PS-*block*-PDMS micelles were decomposed into unimers above about 75°C. The solutions were first kept at 85°C for 2 h to be completely decomposed into unimers and then, quenched to 12°C. After leaving the solutions at 12°C for 1 h for the sake of stabilization, the light-scattering measurements were carried out as a function of temperature under stepwise heating at the rate of 3°C h^{-1}, i.e., repeating 30-min measurements at constant temperatures and increasing temperature.

RESULTS AND DISCUSSION

Three temperature regions in micellization

Figure 1 shows the scattered-light intensity $I^{30°}$ at the scattering angle $\theta = 30°$ as a function of temperature for seven different concentrations on heating at the rate of 3°C h^{-1}. At the highest concentration $C = 8.06 \times 10^{-3}$ g (g of solution)$^{-1}$, the temperature dependence of the scattered-light intensity indicates the existence of two distinct temperature regions other than a unimer region. The scattered-light intensity in the region ranging from 10°C to 60°C slightly decreases with increasing temperature and is about one or two orders of magnitude larger than that in the unimer region. As the temperature increases further, the scattered-light intensity starts to increase abruptly around 66°C, and reaches a maximum value of about 10 times higher than that at room temperature. Then, the scattered-light intensity decreases quickly around 72°C and approaches the value of the unimer region. These two characteristic temperatures, 72°C and 66°C, are here denoted as T_1 and T_2 in order of higher temperature, respectively. At the concentration $C = 3.72 \times 10^{-3}$ g (g of solution)$^{-1}$, these characteristic temperatures T_1 and T_2 correspond to 69°C and 57°C, respectively. The important point to notice at this concentration is that there exists another region at lower temperatures where higher scattered-light intensity is detected. The temperature separating the lower temperature region from the intermediate region is coded T_3, corresponding to 24°C at the concentration $C = 3.72 \times 10^{-3}$ g (g of solution)$^{-1}$. At the concentration $C = 1.90 \times 10^{-3}$ g (g of solution)$^{-1}$, T_1, T_2 and T_3 correspond to 66°C, 48°C and 30°C, respectively.* All of the three temperatures can be assigned in the concentration region of 4.10×10^{-4} g (g of solution)$^{-1} \leq C \leq 3.72 \times 10^{-3}$ g (g of solution)$^{-1}$. However, the peak of

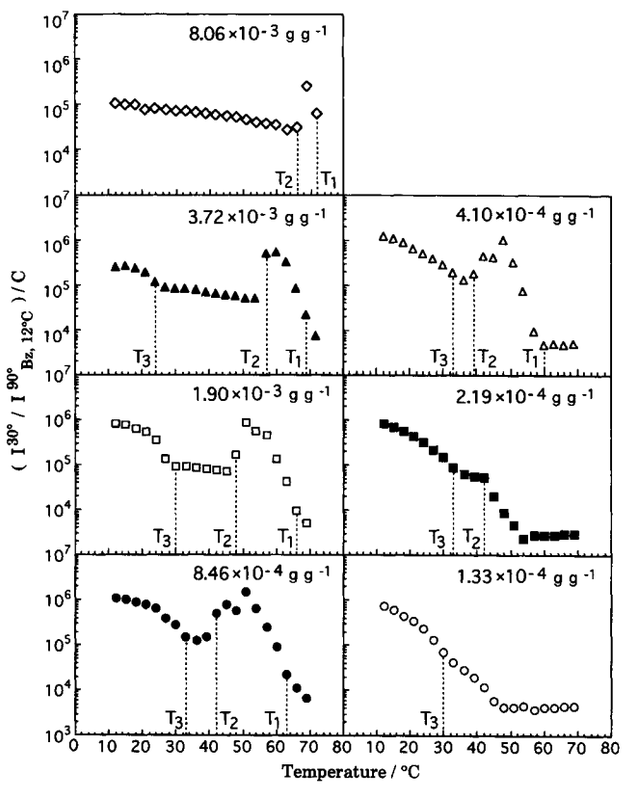

Figure 1 Temperature dependence of scattered-light intensity at an angle of 30° for various concentrations. The scattered-light intensity is displayed as a relative intensity to that of benzene measured at an angle of 90° at 12°C for unit concentration $[(I^{30°}/I^{90°}_{BZ,\ 12°C})/C]$. Characteristic temperatures at which the scattered-light intensity abruptly changes are denoted T_1, T_2 and T_3 in order of higher temperature

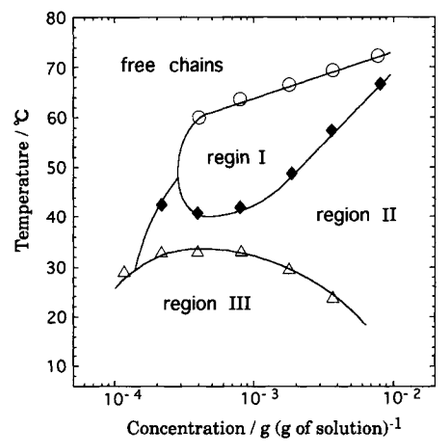

Figure 2 Temperature-concentration diagram of PS-*block*-PDMS in C8/MCH under heating at the rate of 3°C h^{-1} after quenching the solution from 85°C to 12°C. Three distinct regions are illustrated by plotting the characteristic temperatures T_1 (○), T_2 (♦) and T_3 (△) against the polymer concentrations. The border line between region II and unimer region was drawn, on the basis of the simple theory[1] that the c.m.c. increases with increasing temperature, so as to pass through the experimental point of 2.19×10^{-4} g (g of solution)$^{-1}$ and 42°C

*T_1 is here defined as a temperature at which the scattered-light intensity reaches that of the unimer region. In most cases, temperature dependence of the intensity at an angle of 30° was used, while in the case of high concentrations ($C = 8.06 \times 10^{-3}$–1.90×10^{-3} g (g of solution)$^{-1}$), the intensities at relatively higher angles were used for a better determination of T_1 because a little excess intensity of scattered light remains at lower angles even at higher temperatures since micelles require additional time to be completely decomposed into unimers. This is the reason why the intensity at T_1 for the higher concentrations shown in *Figure 1* is higher than that of the unimer region.

Table 1 Static and dynamic properties of micelles in region I for different concentrations

Concentration (10^{-4} g (g of solution)$^{-1}$)	Temperature (°C)	M_{wapp}* (10^7 g mol^{-1})	R_{gapp}* (nm)	R_{happ} (nm)	$\mu_2/\bar{\Gamma}^2$	R_{gapp}/R_{happ}
4.10	42	4.70	71.9	81.5	0.13	0.88
4.10	45	3.89	78.0	103	0.17	0.76
8.46	45	8.77	66.4	72.6	0.15	0.91
8.46	48	5.99	62.6	71.1	0.23	0.88
19.0	51	12.8	86.1	91.8	0.20	0.94
19.0	54	99.0	92.4	102	0.20	0.90
37.2	57	23.0	108	125	0.30	0.87

*Determined by the scattering function of a spherical model fitted to the data points

intensity at higher temperatures is not observed at the lower concentration $C = 2.19 \times 10^{-4}$ g (g of solution)$^{-1}$. Subsequently, at the lowest concentration $C = 1.33 \times 10^{-4}$ g (g of solution)$^{-1}$, T_1 and T_3 merge together and the temperature region of $T_2 < t < T_1$ is not observed.

It follows from the temperature dependence of scattered-light intensity that there exist the three characteristic temperature regions ($T_2 \leq t < T_1$, $T_3 \leq t < T_2$, and $t < T_3$) other than the unimer region ($T_1 \leq t$), with T_1, T_2, and T_3 depending on the concentration. *Figure 2* is a temperature–concentration diagram, where T_1, T_2 and T_3 are plotted against the concentrations, illustrating the three distinct regions designated here as region I, region II and region III, respectively. In the following sections we will describe properties of the micellar solution in the three regions.

In region I (anomalous-micelle region)

In region I ($T_2 \leq t < T_1$), the scattered-light intensity was very high, giving an opalescence, and increased with lapse of time. A milky precipitate eventually appeared in a few days. The observed high intensity must be due to the anomalous micellization often observed near the c.m.t.[23,24]. The precipitate was translucently bluish-white, and its amount was small, almost independent of the concentration and temperature. In other words, the lever rule does not hold in this phenomenon. In *Table 1* are summarized static and dynamic properties in region I. M_{wapp} and R_{happ} are maximally about 1×10^8 g mol^{-1} and 1×10^2 nm, respectively. The ratio of R_{gapp}/R_{happ} is less than unity, suggesting that the shape of the particles is spherical. The polydispersity index $\mu_2/\bar{\Gamma}^2$ ranged from 0.1 to 0.3. These values are relatively larger than those in other regions to reflect the polydispersity of particle size since the apparent diffusion coefficient D_{app} is independent of the $R_{gapp}q$, as shown in *Figure 3a*. The fact that the D_{app} is not dependent on the $R_{gapp}q$ even in the range of $R_{gapp}q > 1$ supports the idea of the spherical structure of the particles. In *Figure 4* the particle-scattering function $P_{app}(q)$ is compared with those of some structures, namely sphere, hollow sphere, disc and rigid rod[29]. The observed $P_{app}(q)$ is closest to that of the sphere model in all cases. This is also consistent with the above results.

This anomalous micellization has been discussed in many papers[1,3,23–25,30] and interpreted in several ways to be attributed to the formation of large micelles, phase separation of impurities, or phase separation of bulk block

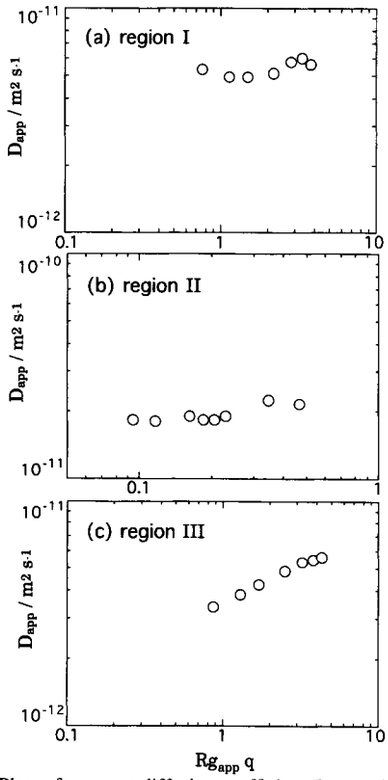

Figure 3 Plots of apparent diffusion coefficient D_{app} against $R_{gapp}q$ at the concentration $C = 1.90 \times 10^{-3}$ g (g of solution)$^{-1}$. The temperatures are 51°C, 30°C and 12°C from the top to the bottom, corresponding to region I (a), region II (b) and region III (c), respectively

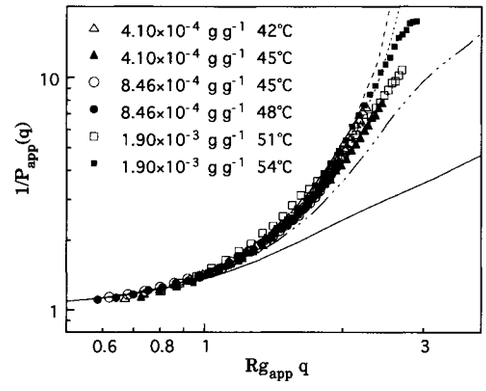

Figure 4 Plots of apparent scattering functions P_{app} of micelles formed in region I against $R_{gapp}q$ compared with values calculated by some simple models, uniform sphere (· · ·), hollow sphere with an infinity-thin shell (- - -), infinity-thin disc (– · · · –) and rigid rod with infinity-thin thickness (————). The plots are for the solutions of $C = 4.10 \times 10^{-4}$ g (g of solution)$^{-1}$ at 42°C (△) and at 45°C (▲), $C = 8.46 \times 10^{-4}$ g (g of solution)$^{-1}$ at 45°C (○) and at 48°C (●), and $C = 1.90 \times 10^{-3}$ g (g of solution)$^{-1}$ at 51°C (□) and at 54°C (■)

Table 2 Static and dynamic properties of micelles in region II at 36°C

M_w (10^7 g mol^{-1})	R_g (nm)	A_2 (10^{-5} cm^3 mol g^{-2})	R_h (nm)	$\mu_2/\bar{\Gamma}^2$	R_g/R_h
1.66	19.0	1.59	22.0	< 0.1	0.862

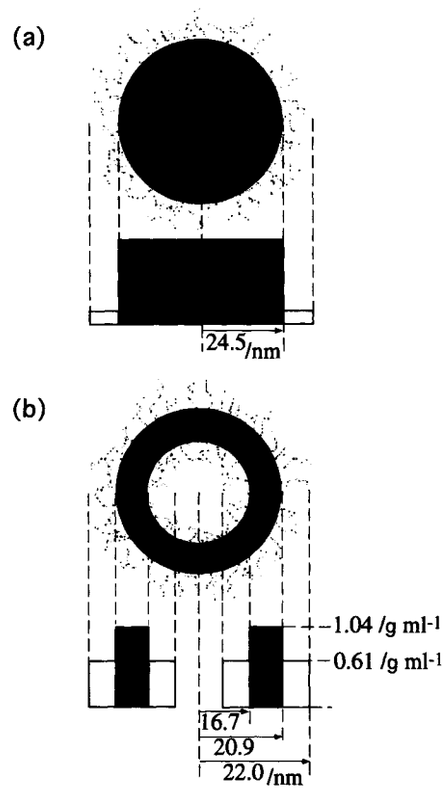

Figure 5 Schematic representation of estimated micellar structures formed in region II at 36°C. (a) a core–corona micelle with uniform segment density , (b) a vesicle. The structure (b) is realistic

copolymers, etc. In the present case, what one can say is that, in region I, large spherical particles are formed and grow, and eventually precipitate, and the phenomenon is not a simple phase separation because of the breakdown of the lever rule.

In region II (spherical-micelle region)

In region II ($T_3 \leq t < T_2$), no changes with time in the intensity and the auto-correlation function of scattered light and no precipitation were observed for more than a week. Characteristic values measured by static and dynamic light-scattering are listed in *Table 2*. These values did not markedly change with concentrations and temperatures except near c.m.c. or c.m.t. The polydispersity index $\mu_2/\bar{\Gamma}^2$ in region II is less than 0.1 in a whole range of concentrations and temperatures, which is smaller than those in other regions showing narrow particle-size distribution. The formed micelle is considered to be spherical because of the ratio of R_g/R_h being less than unity. In region II, the R_g is so small that the range of $R_g q$ is less than unity even at the largest scattering angle of 120° and the $R_g q$ dependence of the D_{app} and the $P_{app}(q)$ are not a useful indication of the structure of the micelle. To estimate the most probable structure of the micelle from the measured values of M_w, R_g and R_h, we suppose two spherical models with uniform segment density; a core–corona micelle and a vesicle, which are illustrated in *Figure 5*. In the case of the core–corona micelle, the radius r_0 of core is estimated from $r_0 = (5/3)^{1/2} R_{g\,core}$, assuming the isorefractivity for the PDMS corona to be 24.5 nm. This value is obviously larger than the measured R_h, 22.0 nm, and even larger than the fully extended length of the PS-block chain, 18.9 nm, calculated from a planar zig-zag with the length of monomer unit being 2.52 Å. Therefore, the core–corona model is not possible. A more likely structure may be the vesicle. The inside radius r_1 of core and the outside radius r_0 of core are estimated from the simultaneous equations of $M_{w\,core} = N_A \rho (4/3)\pi (r_0^3 - r_1^3)$ and $R_{g\,core}{}^2 = (3/5)(r_0^5 - r_1^5)/(r_0^3 - r_1^3)$ with the experimental values of the core-part M_w and R_g, where ρ is the density of bulk PS (1.04 g cm^{-3})[31,32] and $M_{w\,core}$ is given as $M_{w\,core} = M_w \times$ (*PS-block composition*). The values of r_1 and r_0 are calculated to be 16.7 nm and 20.9 nm, respectively. The value of r_0 is quite consistent with the measured R_h, 22.0 nm, if the presence of corona chains is taken into account. Not many cases have been reported, where vesicles are formed by diblock copolymers[33].

In region III (cylindrical-micelle region)

The intensity, accordingly $M_{w\,app}$, in region III ($t < T_3$) decreases with increasing the temperature as shown in *Figure 1*. $R_{g\,app}$ and $R_{h\,app}$ also decrease with increasing temperature. The scattered-light intensity reaches a very high value at 12°C immediately after quenching the solutions from 85°C and exhibits no remarkable time evolution, and no precipitate is detected at 12°C or even at 0°C for several days in contrast with the anomalous micellization. The static and dynamic properties of micelles formed at 12°C are summarized in *Table 3*, where a set of

Table 3 Static and dynamic properties of micelles in region III at 12°C for different concentrations

Concentration (10^{-4} g (g of solution)$^{-1}$)	$M_{w\,app}$ (10^7 g mol^{-1})	$R_{g\,app}$ (nm)	$R_{h\,app}$ (nm)	$\mu_2/\bar{\Gamma}^2$	$R_{g\,app}/R_{h\,app}$
1.33	11.5	94.1	58.2	0.14	1.62
2.19	13.1	100	60.6	0.15	1.65
4.10	25.0	146	80.8	0.20	1.80
8.46	22.2	161	96.8	0.20	1.67
19.0	14.8	138	73.3	0.23	1.89
37.2	3.34	47.6	30.8	0.20	1.54
80.6	1.32	—	19.3	0.07	—

data for the solution of $C = 8.06 \times 10^{-3}$ g (g of solution)$^{-1}$ at 12°C in region II is also listed for comparison. M_{wapp}, R_{gapp} and R_{happ} at concentrations around 1×10^{-3} g (g of solution)$^{-1}$ are much larger than those in region II, respectively. The ratio of R_{gapp}/R_{happ} is more than unity, which shows that the shape of micelles is not spherical. As shown in *Figure 3c*, the apparent diffusion coefficient D_{app} depends on the R_{gapp} in region III while the D_{app} in region I and region II is independent of $R_{gapp}q$ even in a q-range of $R_{gapp}q > 1$, so the shape of the micelles is anisotropic in region III. Furthermore, the particle-scattering function $P_{app}(q)$ is very close to that of a thin-rod model as shown in *Figure 6*, where the observed $P_{app}(q)$ is compared with those of some structural models[29]. It follows from these observations that cylindrical micelles may be formed in region III. The polydispersity index $\mu_2/\bar{\Gamma}^2$ ranges from 0.1 to 0.2 over the concentration 1.33×10^{-4} g (g of solution)$^{-1}$ $\leq C \leq$ 3.72×10^{-3} g (g of solution)$^{-1}$. The relatively large $\mu_2/\bar{\Gamma}^2$ value may be attributed to the broader particle-size distributions at the concentration $C = 3.72 \times 10^{-3}$ g (g of solution)$^{-1}$ probably because the concentration is near the boundary between region II and region III, while it may be attributed to the internal motions of non-spherical micelles, at least partially, at other concentrations where $R_{gapp}q > 1$. In the following, the most probable structure of the cylindrical micelle will be estimated from the measured values of $M_{w\,app}$, $R_{g\,app}$ and R_{happ}.

First, assuming the uniform density in a cylinder, we evaluate the contour length of the cylindrical micelle from the experimental values of M_{wapp} and R_{gapp}. The diameter of the core is taken to be equal to the unperturbed end-to-end distance L_0 of the PS-block chain, which is calculated to be 6.56 nm, from the characteristic segment length $L_0/N^{0.5} = 0.757$ nm[34] with the degree of polymerization $N = 75$. Using this value of the core diameter L_0, the contour length L of the cylindrical micelle is evaluated by

$$Mw_{core} = N_A \rho \pi \left(\frac{L_0}{2}\right)^2 L \tag{8}$$

to be $L = 5.0 \times 10^3$ nm for the solution of $C = 1.90 \times 10^{-3}$ g (g of solution)$^{-1}$ at 12°C. The persistence length P can be estimated from R_{gapp} with the obtained L, using the formula for a worm-like chain[35,36]:

$$R^2_{gcore} = P^2\left[\frac{L}{3P} - 1 + \frac{2P}{L} - \frac{2\{1-\exp(-L/P)\}}{(L/P)^2}\right] \tag{9}$$

The obtained value of P is 11.7 nm, which is comparable to twice of the core diameter L_0 and is too small for the persistence length of the micelle. If the L_0 is assumed to be equal to the core *radius*, instead of the diameter, it may safely be concluded that the calculated value of $P =$ 52.5 nm is still too short as the persistence length of the micelle, compared with the core diameter $2L_0 = 13.1$ nm and the contour length $L = 1.2 \times 10^3$ nm. Therefore, the model of a cylinder with uniform density can not reasonably reproduce the experimental values of M_{wapp} and R_{gapp} and is not appropriate for the model of the present micelle. The above result of calculation suggests that the micelle in region III could be a hollow cylinder since the spherical micelle in region II is hollow.

Then, assuming a hollow cylinder with a pair of hollow hemispheres at its ends for the micellar structure, we evaluate the contour length and the radius of the cylindrical micelle to reproduce the experimental values of M_{wapp} and R_{gapp}. For a rigid hollow hemispherical cylinder with the inside radius r_1, the outside radius r_0, and the length of cylinder L excluding the hemisphere parts, M_{wcore} and R_{gcore} are respectively expressed as

$$M_{wcore} = N_A \rho\left[\frac{4}{3}\pi\{r_0^3 - r_1^3\} + \pi L\{r_0^2 - r_1^2\}\right] \tag{10}$$

$$R^2_{gcore} = \frac{\frac{4}{5}(r_0^5 - r_1^5) + L(r_0^4 - r_1^4) + \frac{L^2}{3}(r_0^3 - r_1^3) + \frac{L^3}{3}(r_0^2 - r_1^2)}{\frac{4}{3}(r_0^3 - r_1^3) + L(r_0^2 - r_1^2)} \tag{11}$$

The r_0 and L can be obtained from equations (10) and (11) with the experimental values of M_{wcore} and R_g and the thickness $r_0 - r_1$ of the core of the hollow cylindrical micelle being assumed equal to that of the vesicle in region II, i.e. $r_0 - r_1 = 4.2$ nm. Moreover, to examine the reality of obtained values of r_0 and L, we compare the observed R_{happ} with the value calculated from these values by using Norisuye's formula[37] for a rigid hemispherical cylinder:

$$\frac{L_t/2}{R_h} = \ln\frac{2L_t - 2R + \{4L_t^2 - 4L_t(2R) + 2(2R)^2\}^{1/2}}{2R} + \tag{12}$$

$$\frac{L_t + 2^{1/2}(2R) - \{4L_t^2 - 4L_t(2R) + 2(2R)^2\}^{1/2}}{L_t} +$$

$$\{(2R)/2L_t\}\ln\frac{(2^{1/2}-1)^2\left[2R + \{4L_t^2 - 4L_t(2R) + 2(2R)^2\}^{1/2}\right]}{2L_t - 2R + \{4L_t^2 - 4L_t(2R) + 2(2R)^2\}^{1/2}}$$

where R is the hydrodynamic radius of the cylinder including corona and L_t is the total contour length ($L + 2R$). Assuming the hydrodynamic thickness of the outside corona of the hollow cylindrical micelle equal to that of the vesicle in region II, i.e. $R - r_0 = 1.1$ nm, we evaluate the R_h by equation (12) with the values of r_0 and L obtained by equations (10) and (11). The calculated values of r_0, L_t, the axis ratio $(L + 2r_0)/2r_0$ and R_h at 12°C are listed in *Table 4*. The axis ratio is relatively short, so that the

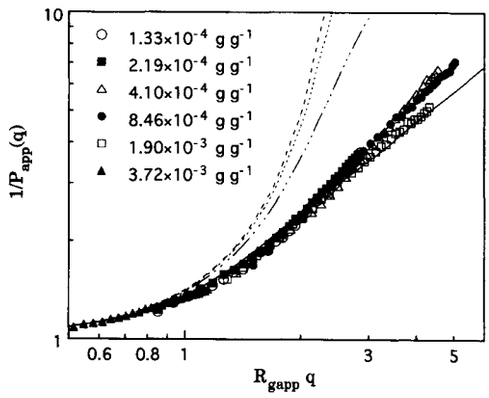

Figure 6 Plots of apparent scattering functions P_{app} of micelles formed in region III at 12°C against $R_{gapp}q$ compared with values calculated by some simple models, uniform sphere (· · ·), hollow sphere with an infinity-thin shell (- - -), infinity-thin disc (– · · · –) and rigid rod with infinity-thin thickness (————). The concentrations are 1.33×10^{-4} g (g of solution)$^{-1}$ (○), 2.19×10^{-4} g (g of solution)$^{-1}$ (■), 4.10×10^{-4} g (g of solution)$^{-1}$ (△), 8.46×10^{-4} g (g of solution)$^{-1}$ (●), 1.90×10^{-3} g (g of solution)$^{-1}$ (□) and 3.72×10^{-3} g (g of solution)$^{-1}$ (▲)

Table 4 Calculated values of micelles formed in region III at 12°C for different concentrations

Concentration (10^{-4} g (g of solution)$^{-1}$)	r_0 (nm)	L_t (nm)	$(L + 2r_0)/2r_0$	calc. R_h (nm)
1.33	17.5	328	9.31	62.0
2.19	18.6	349	9.34	65.9
4.10	23.6	505	10.6	90.9
8.46	19.3	562	14.5	91.8
19.0	15.4	487	15.8	77.5
37.2	11.0	168	7.56	34.6

approximation of a *rigid* micelle is not bad. Agreements of the calculated values of R_h with the experimental values of R_{happ} are reasonably good, and therefore the hollow cylindrical micelles of these sizes are considered to be formed in region III.

It should be noticed, by comparing micelles formed in region II and region III, that micelles with a larger association number appear at lower concentrations in the present system. In most cases of diblock-copolymer micellar solutions, micelles with a larger association number are formed at higher polymer concentrations, although there are a few exceptions, for instance, PS-*block*-PB solution in *n*-decane studied by Tsunashima[13]. We suspect that the larger micelles appearing at lower concentrations are not stable ones at equilibrium, but are temporarily formed in the course of the micellization process. In fact, we have experimental results that indicate process dependence of micellar structure in region III. That is, as shown in *Figure 7*, the larger micelles are formed on the heating process only, but, on cooling from region II, the scattered-light intensity exhibits a monotonical slight increase with decreasing temperature, which may imply no change of micellar shape from a small sphere. Process-dependent micellar structure, which is different between heating and cooling processes, was reported for micellar solutions prepared by dissolution of bulk diblock copolymers in a micellar temperature region[38–41]. This phenomenon looks similar to our observation, but the situation is totally different. In the present case, the solutions were first completely decomposed in the unimer region, which was the starting solution for both heating and cooling experiments.

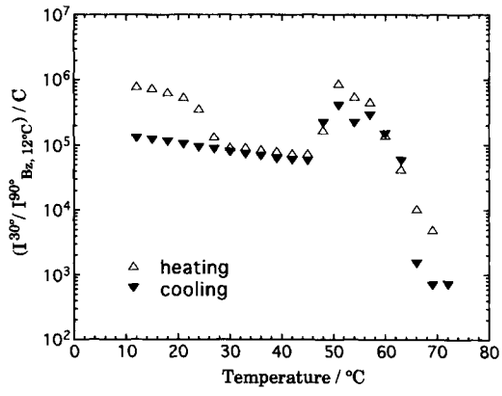

Figure 7 Temperature dependence of the scattered-light intensity at an angle of 30° at the concentration $C = 1.90 \times 10^{-3}$ g (g of solution)$^{-1}$ on heating (△), as shown in *Figure 1*, and on cooling from 72°C down to 12°C (▼). The scattered-light intensity is displayed as a relative intensity to that of benzene measured at an angle of 90° at 12°C for unit concentration $[(I^{30°}/I^{90°}_{BZ,12°C})/C]$. The increase in the scattered-light intensity at lower temperatures was not observed during the cooling process

Therefore, the difference between heating and cooling processes comes from the difference in temperature history of the solution in the course of micellization from unimer or micelle-to-micelle rearrangement. It is not directly observed here, but is speculated that larger micelles appear at a shorter time regime before formation of equilibrium micelles in a micellization process, and that the size of micelles does not always increase monotonically, involving the change of micellar structure in the course of micellization.

CONCLUSIONS

The present micellar solution of PS-*block*-PDMS in the selective solvent C8/MCH has three different temperature–concentration regions other than a unimer region, as illustrated in *Figure 2*. Region I at higher temperatures below the unimer region is the so-called anomalous-micellization region, where large spherical particles are formed and grow, and eventually precipitate in a few days. We suppose it is not a simple phase separation. In region II at intermediate temperatures, stable vesicles are formed at any temperatures and concentrations unless close to c.m.c. or c.m.t. Region III at lower temperatures and lower concentrations is the cylindrical micelle region. The micellar structure in region III is estimated to be a rigid hollow cylinder, and these micelles are not formed during the cooling process. The path of the temperature, or in other words, the difference in the course of micellization processes has a significant influence on the observed structure of micelles.

REFERENCES

1. Tuzar, Z. and Kratochvíl, P., in *Surface and Colloid Science*, Vol. 15, ed. E. Matijević. Plenum Press, New York, 1993, p. 1.
2. Tuzar, Z. and Kratochvíl, P., *Makromol. Chem.*, 1972, **160**, 301.
3. Chu, B., Zhou, Z. and Wu, G., *J. Non-Crystal. Solids*, 1994, **172-174**, 1094.
4. Chu, B., *Langmuir*, 1995, **11**, 414.
5. Elias, H. -G., in *Light Scattering from Polymer Solutions*, ed. M. B. Huglin. Academic Press, London, 1972, p. 397.
6. Leibler, L., Orland, H. and Wheeler, J. C., *J. Chem. Phys.*, 1983, **79**, 3550.
7. Zhou, Z., Chu, B. and Peiffer, D. G., *Macromolecules*, 1993, **26**, 1876.
8. Quintana, J. R., Villacampa, M. and Katime, I. S., *Macromolecules*, 1993, **26**, 601.
9. Quintana, J. R., Villacampa, M. and Katime, I. S., *Macromolecules*, 1993, **26**, 606.
10. Honda, C., Sakaki, K. and Nose, T., *Polymer*, 1994, **35**, 5309.
11. Gao, Z. and Eisenberg, A., *Macromolecules*, 1993, **26**, 7353.
12. Tsunashima, Y., Hirata, M. and Kawamata, Y., *Macromolecules*, 1990, **23**, 1089.
13. Tsunashima, Y., *Macromolecules*, 1990, **23**, 2963.

14. Mortensen, K. and Pedersen, J. S., *Macromolecules*, 1993, **26**, 805.
15. Mortensen, K., Brown, W. and Jørgensen, E., *Macromolecules*, 1994, **27**, 5654.
16. Noolandi, J., Shi, A. -C. and Linse, P., *Macromolecules*, 1996, **29**, 5907.
17. Linse, P., *J. Phys. Chem.*, 1993, **97**, 13896.
18. Linse, P., *Macromolecules*, 1994, **27**, 2685.
19. Fleischer, G., *J. Phys. Chem.*, 1993, **97**, 517.
20. Schillén, K., Brown, W. and Koňák, Č., *Macromolecules*, 1993, **26**, 3611.
21. Schillén, K., Brown, W. and Johnsen, R. M., *Macromolecules*, 1994, **27**, 4825.
22. Zhou, Z. and Chu, B., *Macromolecules*, 1994, **27**, 2025.
23. Zhou, Z. and Chu, B., *Macromolecules*, 1988, **21**, 2548.
24. Zhou, Z. and Chu, B., *Macromolecules*, 1987, **20**, 3089.
25. Sikora, A. and Karasz, F. E., *Macromolecules*, 1993, **26**, 177.
26. Ehl, P. J., Loucheux, C., Reiss, C. and Benoit, H., *Makromol. Chem.*, 1964, **75**, 35.
27. Kratochvíl, P., Deželić, Gj. and Kerker, M., *J. Polym. Sci.*, 1965, **A3**, 2259.
28. Gulari, E. and Chu, B., *Biopolym.*, 1979, **18**, 2943.
29. Burchard, W., in Light scattering from polymers, *Adv. Polym. Sci.*, 48, eds. W. Burchard and G. D. Patterson. Springer-Verlag, Berlin, 1983, p. 1.
30. Utiyama, H., Takenaka, K., Mizumori, M., Fukuda, M., Tsunashima, Y. and Kurata, M., *Macromolecules*, 1974, **7**, 515.
31. Natta, G., *J. Polym. Sci.*, 1955, **16**, 143.
32. R. H. Boundy and R. F. Boyer, eds., *Styrene, Its Polymers, Copolymers and Derivatives*. Reinhold Publishing Corp., New York, 1952.
33. Hilfiker, R., Wu, D. Q. and Chu, B., *J. Colloid Interface Sci.*, 1990, **135**, 573.
34. Miyaki, Y., Einaga, Y. and Fujita, H., *Macromolecules*, 1978, **11**, 1180.
35. Tracy, M. A. and Pecora, R., *Annu. Rev. Phys. Chem.*, 1992, **43**, 525.
36. Allison, S. A., Sorlie, S. S. and Pecora, R., *Macromolecules*, 1990, **23**, 1110.
37. Norisuye, T., Motowoka, M. and Fujita, H., *Macromolecules*, 1979, **12**, 320.
38. Price, C., Chan, E. K. M., Hudd, A. L. and Stubbersfield, R. B., *Polymer*, 1986, **27**, 196.
39. Stejskal, J., Hlavatá, D., Sikora, A., Koňák, Č., Pleštil, J. and Kratochvíl, P., *Polymer*, 1992, **33**, 3675.
40. Stejskal, J., Koňák, Č., Helmstedt, M. and Kratochvíl, P., *Collect. Czech. Chem. Commun.*, 1993, **58**, 2282.
41. Hlavatá, D., Stejskal, J., Pleštil, J., Koňák, Č., Kratochvíl, P., Helmstedt, M., Mio, H. and Laggner, P., *Polymer*, 1996, **37**, 799.